

Article

Design of Multi-Objective-Based Artificial Intelligence Controller for Wind/Battery-Connected Shunt Active Power Filter

Srilakshmi Koganti ¹, Krishna Jyothi Koganti ² and Surender Reddy Salkuti ^{3,*} 

- ¹ Department of Electrical and Electronics Engineering, Sreenidhi Institute of Science and Technology, Hyderabad, Telangana 501301, India; kslakshmi@sreenidhi.edu.in
- ² Department of Computer Science and Engineering, Geethanjali College of Engineering and Technology, Hyderabad, Telangana 501301, India; drkrishnajyothi.cse@gcet.edu.in
- ³ Department of Railroad and Electrical Engineering, Woosong University, Daejeon 34606, Korea
- * Correspondence: surender@wsu.ac.kr

Abstract: Nowadays, the integration of renewable energy sources such as solar, wind, etc. into the grid is recommended to reduce losses and meet demands. The application of power electronics devices (PED) to control non-linear, unbalanced loads leads to power quality (PQ) issues. This work presents a hybrid controller for the self-tuning filter (STF)-based Shunt active power filter (SHAPF), integrated with a wind power generation system (WPGS) and a battery storage system (BS). The SHAPF comprises a three-phase voltage source inverter, coupled via a DC-Link. The proposed neuro-fuzzy inference hybrid controller (NFIHC) utilizes both the properties of Fuzzy Logic (FL) and artificial neural network (ANN) controllers and maintains constant DC-Link voltage. The phase synchronization was generated by a self-tuning filter (STF) for the effective working of SHAPF during unbalanced and distorted supply voltages. In addition, STF also does the work of low-pass filters (LPFs) and HPFs (high-pass filters) for splitting the Fundamental component (FC) and Harmonic component (HC) of the current. The control of SHAPF works on d-q theory with the advantage of eliminating low-pass filters (LPFs) and phase-locked loop (PLL). The prime objective of the projected work is to regulate the DC-Link voltage during wind uncertainties and load variations, and minimize the total harmonic distortion (THD) in the current waveforms, thereby improving the power factor (PF). Test studies with various combinations of balanced/unbalanced loads, wind velocity variations, and supply voltage were used to evaluate the suggested method's superior performance. In addition, the comparative analysis was carried out with those of the existing controllers such as conventional proportional-integral (PI), ANN, and FL.

Keywords: power quality; wind power; battery storage; fuzzy logic; total harmonic distortion; power factor; artificial neural network



Citation: Koganti, S.; Koganti, K.J.; Salkuti, S.R. Design of Multi-Objective-Based Artificial Intelligence Controller for Wind/Battery-Connected Shunt Active Power Filter. *Algorithms* **2022**, *15*, 256. <https://doi.org/10.3390/a15080256>

Academic Editor: Abdulsalam Yassine

Received: 22 June 2022

Accepted: 22 July 2022

Published: 25 July 2022

Publisher's Note: MDPI stays neutral with regard to jurisdictional claims in published maps and institutional affiliations.



Copyright: © 2022 by the authors. Licensee MDPI, Basel, Switzerland. This article is an open access article distributed under the terms and conditions of the Creative Commons Attribution (CC BY) license (<https://creativecommons.org/licenses/by/4.0/>).

1. Introduction

The power distribution network is subjected to higher PQ problems such as voltage sag/swell/disturbance, harmonics, PF, interruptions, flickers, etc. when compared to the generation and transmission side due to the integration of PED and nonlinear loads.

1.1. Challenges and Motivation

The increase in the application of large non-linear industrial loads has led to an increase in harmonic currents thereby reducing PF. Electricity with a bad quality is dangerous and uneconomical at both the utility and consumer end. Therefore, maintaining PQ became a challenge to power engineers. The regulation of capacitor voltage across the DC-Link in addition to minimization of THD in current waveforms and improving PF motivated the invention of a new hybrid controller. To improve the PQ, the FACTS device used at the distribution side of the utility grid is the SHAPF.

1.2. Literature Review

The SHAPF configurations for 1- ϕ and 3- ϕ with three and four-wire systems configurations along with the compensation methods for both sinusoidal/non-sinusoidal supply voltage conditions were reviewed. Additionally, the latest advancements and practical applications of SHAPF for future study were also discussed [1]. The SRFT-based new controller was developed to mitigate the PQ issues through the 3 ϕ -4wire UPQC for unbalanced and distorted loads of the distribution network [2].

The performance of the SHAPF was analyzed under balanced/unbalanced conditions with the hybridization of both the superior properties of the FL controller and PI controller to diminish THD [3]. A novel self-tuning perturb and observe technique-based solar battery integrated SHAPF was designed to minimize the THD and manage the reactive power effectively. In addition, a maximum Kalman filter was employed for the effective reference current estimation [4]. Moreover, the advancement in artificial intelligence systems such as FL and ANN controller was able to control the SHAPF effectively to reduce PQ issues during dynamic non-linear load changes [5–7].

The PV-connected UPQC was designed and its performance was studied under various load distortions by extracting maximum power to reduce THD and improve performance [8]. The fuel cell-supported SHAPF with SRFT-based PI controller was designed to maintain DC-link voltage and minimize THD [9]. The optimal tuning of SHAPF was carried out with the aim of reactive power and THD minimization based on the particle swarm optimization and grey wolf optimization hybridization algorithm along with the fractional proportional integral derivative control technique [10]. The modern smart grid with ANN feed-forward control strategy for wind-solar integrated DSTATCOM was proposed to boost the voltage profile and maintain reactive power at the grid [11].

The novel adaptive-power technique was implemented on the H-bridge eight-switch UPQC with the motive of reducing THD and source voltage-related fluctuations [12]. The PV/wind and PEMFCS connected multi-levels UPQC was proposed with the view of diminishing THD, eliminating sag, swell, voltage distortions, and swell efficiently. In addition, hardware was implemented to analyze the real-time performance of the proposed method [13]. However, to overcome the drawbacks of the conventional PI controller, the Sliding Mode controller was suggested for DSTATCOM to improve the THD and maintain the DC voltage constant during load variations [14]. The modern AC-DC microgrid with the intelligent FL-PI and FL-PID controller was designed with the view of minimizing PQ issues and improving voltage stability. In addition, the performance analysis was carried out with two different case studies with dynamic load changes [15]. The STF-based control for SHAPF was investigated to reduce the use of LPF and PLL, and theoretical and practical analysis was carried out [16].

The FLC was suggested for the UPQC to minimize the distortions in voltage and current waveforms for RL non-linear loads. In addition, a comparative analysis was done with and without UPQC [17]. Furthermore, the novel predictive phase dispersion modulation method was designed for the H-Bridge cascaded Multi-Level UPQC with the prime intention of compensating the voltage distortions, imperfections in current waveforms, and regulating DC-Link capacitor voltage [18]. The UPQC was suggested for the induction-furnace load at a steel plant to reduce current and voltage harmonics. In addition to exhibiting its superior performance, the comparison was done with that of the synchronous compensator [19]. A novel Fourier transform analysis was suggested for the PV, wind, fuel cell, and battery-integrated UPQC intending to eliminate voltage / current THD, sag, swell, and distortions in the supply voltage [20]. The various SVPWM control strategies were discussed for power quality enhancement and comparisons were carried out with the experimental results discussed in the literature [21].

The Internet of Things (IoT)-based power management unit to identify the PQ issues and the implementation of an ANN-based controller was designed for SHAPF to reduce THD [22]. The modern AC-DC microgrid with the intelligent FL-PI and FL-PID controller was designed with the view of minimizing PQ issues and improving voltage stability.

In addition, performance analysis was carried out with two different case studies with dynamic load changes [23]. An adaptive full order observer-based control algorithm was developed for the UPQC to improve the PQ due to its fast response in fault detection for all positive sequence components, and high accuracy in monitoring under all various loads/grid conditions. In addition, a BBO algorithm was employed for the optimal tuning of Kp and Ki values for PIC on UPQC to minimize the DC-Link voltage oscillations [24].

However, the PQ issues for the micro-grid integrated distribution network were addressed using UPQC to mitigate voltage imbalances and current harmonics. An adaptive network-based fuzzy inference system was proposed to maximize the utilization and efficiency of the system [25]. An automated shifting method between the grid and island modes was developed for PV battery integrated UPQC in the view of addressing the PQ issues with low disturbance to the local loads. Further, the system performance was validated with experimental results [26]. The combination of both the improved bat algorithm and moth flame algorithm optimization-based hybrid control technique was developed to address the PQ issues in the micro-grid system in the view of minimizing the error function of power variation. In addition, the operation cost of renewable sources was reduced with the optimal tuning of Kp and Ki parameters [27].

An ANN controller based on a hybrid combination of reactive power control with unit vector template generation was designed for UPQC to mitigate PQ issues effectively. In addition, solar PV is connected to reduce the ratings of the power converters, and stabilize the DC-Link capacitor voltage during faulty and load variation conditions [28]. In addition, the novel sequence-component detection method hybridized with unit vector-template generation was proposed for the double-stage solar integrated UPQC to diminish PQ issues [29]. The review of various topologies, compensation techniques, controllers, and technological advancements in recent years for the UPQC were outlined with the motive of eliminating PQ issues [30].

Furthermore, the novel synchro-squeezing wavelet transform and ANN-based hybrid control algorithm were developed for the shunt controller of distributed generation integrated UPQC to detect and identify and control the PQ events regularly. In addition, a comparison was carried out with the ANN controller [31]. The optimal gain coefficients of modified active-power filter (MAPF) with a power filter compensator-kit (PFCK) were suggested with Harris hawk optimization (HHO), grasshopper optimization algorithm (GOA), artificial bee colony (ABC), and differential evolution (DE) to minimize current and voltage harmonics in addition to the diminishing the controller error [32]. The grid-connected network with an adaptive FL-C based on a series active power filter was designed to address PQ problems such as voltage fluctuations/interruptions, reduction of current harmonics, and maintaining constant DC-Link voltage [33].

1.3. Key Contribution

This study is designed to enhance the PQ in the distribution network. The highlights of this article are emphasized below:

- Design of hybrid controller (NFIHC) involving both the properties of FL and ANN techniques for the WPGS and BS-integrated SHAPF (SH-WPBS).
- The prime aim of the proposed method is to minimize THD thereby improving PF and maintaining constant DC-Link voltage.
- The proposed STF is used to generate synchronization phases (SYP) for SHAPF instead of PLL. In addition, STF also does the work of LPFs and HPFs for splitting the FC of current.
- The results are obtained for variation in loads, distorted supply voltage, and wind uncertainties as case studies.
- Future performance analysis was carried out with PI, FL, and ANN controllers. To exhibit the superiority of the proposed technique, validation was done with those existing methods that are available in the literature.

However, from the literature survey, it is noticed that the majority of research papers focused mainly on THD reduction and or DC-Link voltage regulation as the main objective with the conventional PLL and LPFs. In the proposed work, in addition to THD minimization with DC-Link voltage balancing, PF improvement was also considered an objective with STF instead of PLL and LPFs. Although quite a lot of techniques were recommended in the literature review, there is still a possibility of designing new controllers and techniques for efficiently eliminating PQ problems.

1.4. Paper Organization

Section 2 designs the components of the proposed SHAPF, Section 3 discusses the control-based STF with proposed NFIHC for SHAPF, Section 4 provides results and discussions, and lastly, Section 5 gives the conclusion.

2. Proposed SH-WPBS

Figure 1 gives the construction of SHAPF integrated with a BSS and WPGS. The WPGS and BSS are associated with the SHAPF via a DC-Link and boost converter. This paper presents NFIHC, which utilizes both the properties of FL and ANN. The purpose of SHAPF is to inject a suitable current to minimize the current harmonics thereby making the source current distortion-free and also maintaining the constant DC-link voltage. Different combinations of loads were considered in the proposed work. The proposed SHAPF specifications with loads are exhibited in Table 1.

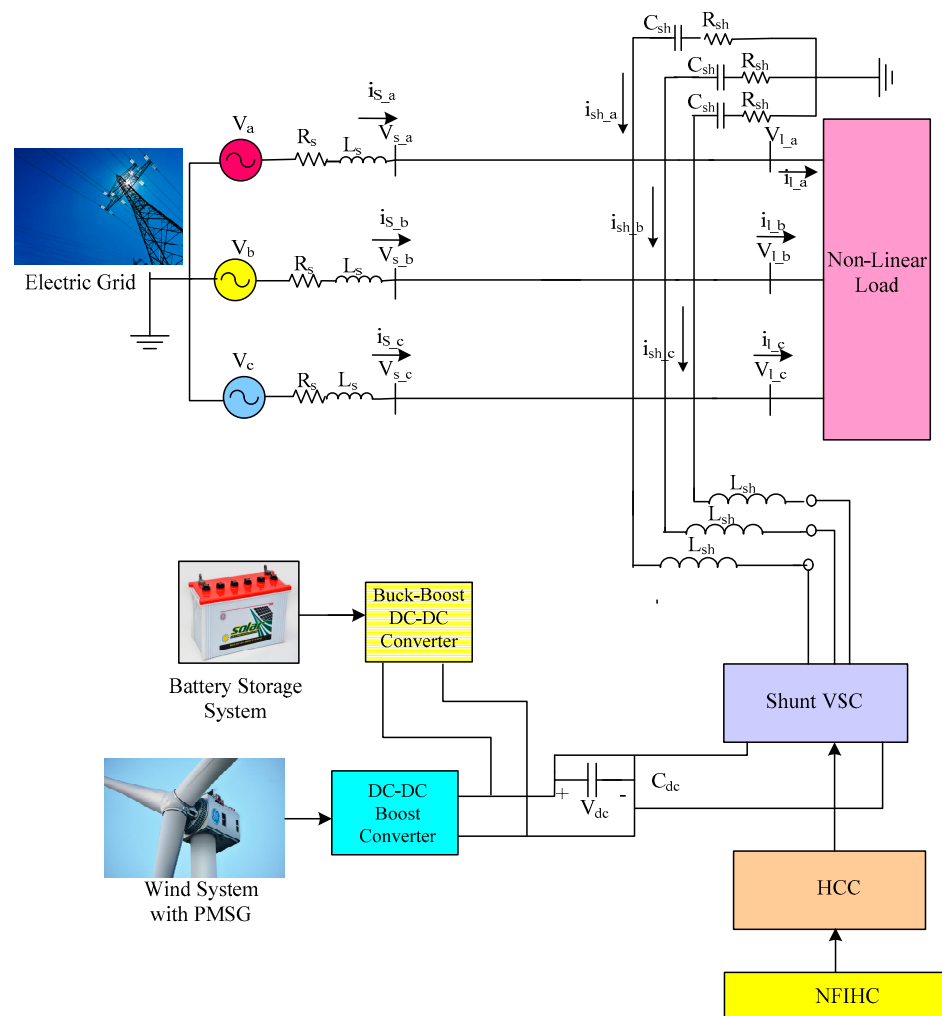


Figure 1. Construction of SH-WPBS.

Table 1. SHAPF specifications and loads.

Component	Rating
Source	V_s : 415 V; f : 50 Hz R_s : 0.10 Ω ; L_s : 0.150 mH
Shunt compensator	R_{sh} : 0.0010 Ω ; L_{sh} : 2.150 mH; C_{sh} : 1.0 μ f hysteresis band: 0.010 A
DC-Link	C_{dc} : 9400.00 μ f; V_{dc} Voltage: 700.0 V

The WPGS and BSS act as external support for the DC-Link via the DC-DC boost converter and buck-boost converters to maintain the constant DC-Link voltage during load variations and minimize PQ issues as shown in Figure 2. The WPGS ratings are given in Table 2. The power equilibrium equation of the projected system at the DC link is given by Equation (1).

$$P_W + P_{BS} - P_{dc} = 0 \tag{1}$$

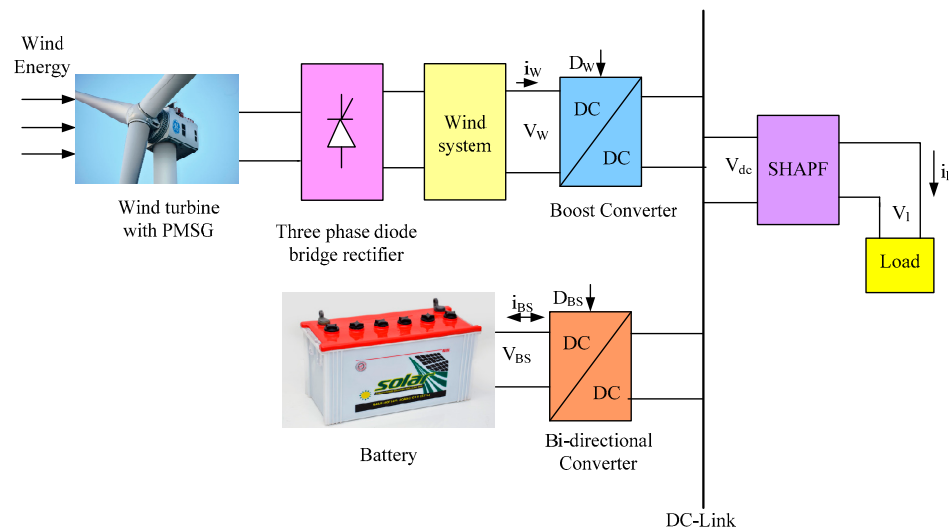


Figure 2. WPGs and BSS connected to DC-Link.

Table 2. WPGS and BSS specifications.

Equipment	Parameter	Rating
	Rated-capacity	400 Ah
	Maximum-capacity	500 Ah
	Nominal-voltage	750 V
	Maximum-voltage	756 V
	Nominal turbine mechanical power	3 MW
	Base wind speed	11 m/s
	Pitch angle controller integral gain	5
	Pitch angle controller proportional gain	25
	Maximum pitch angle	45 deg.
	Maximum rate of change of pitch angle	25 deg./s

2.1. Wind Power Generation System (WPGS)

The WPGS control system consists of a wind turbine, a PMSG, and a boost converter. The power output from the wind system is given by Equation (2)

$$P_w = 12\rho A v^3 C_p(\lambda, \theta) \tag{2}$$

where

ρ is the density of air in kg/m^3

A is the area under swept by the rotor turbine blades in m^2

v is the velocity of the wind in m/s

C_p is the coefficient of power, function of (TSR, λ) and pitch-angle (θ).

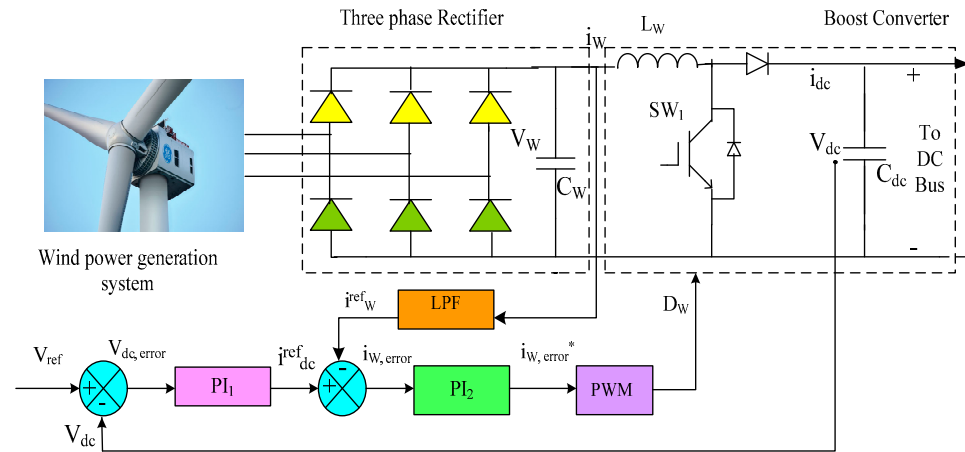


Figure 3. Wind System with controller.

The reference current i_{dc}^{ref} is approximated by reducing the of DC-Link voltage error $V_{dc,err}$ using a PI controller. In mathematical terms, the approximation can be explained as given in Equations (3) and (4). The wind error current reference $i_{W,err}^*$ is obtained by PI of wind error current $i_{W,err}$. Where $i_{W,err}$ is the difference between the reference, the DC-Link current i_{dc}^{ref} and wind current i_W^{ref} obtained from LPF is given in Equations (5)–(7).

$$V_{dc,err}(t) = V_{dc}^{ref} - V_{dc} \tag{3}$$

$$i_{dc}^{ref} = K_{p,1} V_{dc,err}(t) + K_{i,1} \int_0^t V_{dc,err}(t) dt \tag{4}$$

$$i_{W,err}(t) = i_{dc}^{ref} - i_W^{ref} \tag{5}$$

$$i_{W,err}^* = K_{p,2} i_{W,err}(t) + K_{i,2} \int_0^t i_{W,err}(t) dt \tag{6}$$

where

$$i_W^{ref} = \left(\frac{1}{1 + T.S} \right) * i_W \tag{7}$$

$K_{p1} = 1.15$, $K_{i1} = 0.2$, $K_{p2} = 1.477$ and $K_{i2} = 3.077$ are chosen heuristically.

2.2. Battery Storage (BS)

The BS controller consists of a lead-acid battery connected to a bi-directional buck-boost converter. It maintains DC-Link voltage through a PI controller as given in Figure 4. The state-of-charge (SOC) is given by Equation (8).

$$SOC = 100(1 + \int i_{BS} dtQ) \tag{8}$$

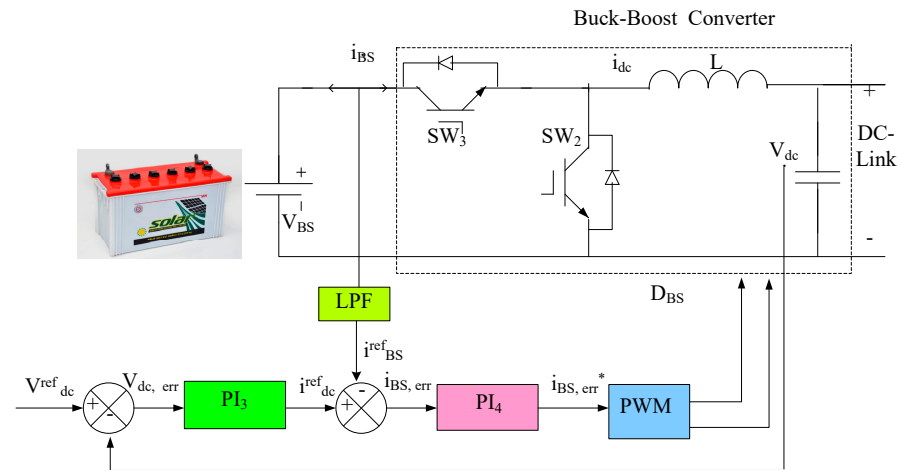


Figure 4. BS controller.

Depending on the amount of power generated by the wind system, the battery operates in charging and discharging modes, satisfying the minimum and maximum constraints, which are determined by Equation (9).

$$SOC_{min} \leq SOC \leq SOC_{max} \tag{9}$$

The reference current i_{dc}^{ref} is approximated by reducing the DC-Link voltage error $V_{dc, err}$ using a PI controller in mathematical terms. The approximation can be explained as given in Equations (10) and (11). The battery error current reference $i_{BS, err}^*$ is obtained by the PI of battery error current $i_{BS, err}$. Where $i_{BS, err}$ is the difference between reference DC-Link current i_{dc}^{ref} and battery current i_{BS}^{ref} given in Equation (12) obtained from LPF given in Equations (13) and (14).

$$V_{dc, err}(t) = V_{dc}^{ref} - V_{dc} \tag{10}$$

$$i_{dc}^{ref} = K_{p,3} V_{dc, err}(t) + K_{i,3} \int_0^t V_{dc, err}(t) dt \tag{11}$$

$$i_{BS, err}(t) = i_{dc}^{ref} - i_{BS}^{ref} \tag{12}$$

$$i_{BS, err}^* = K_{p,4} i_{BS, err}(t) + K_{i,4} \int_0^t i_{BS, err}(t) dt \tag{13}$$

where

$$i_{BS}^{ref} = \left(\frac{1}{1 + T.S} \right) * i_{BS} \tag{14}$$

$K_{p3} = 1.05$, $K_{i3} = 0.01$, $K_{p4} = 1.27$, and $K_{i4} = 3.07$ are chosen heuristically. Table 3 gives the power dispersion at DC-link under various working conditions of the SH-WPBS.

Table 3. Power-sharing at DC-link Bus.

Level of WPG	Action
$WPG > P_{dc}$	Extra power produced by WPG is used to charge BS till it attains SOC_{max}
$WPG = P_{dc}$	WPG alone will supply P_{dc} .
$WPG < P_{dc}$	The power difference is supplied by BS until it reaches SOC_{min}
No WPG	BS alone supplies P_{dc} .

3. Control Strategy

According to the d-q theory to compensate for the current harmonics and the improved power factor, first, they are transformed into Clarke’s reference. Later, the harmonic component (HC) and fundamental component (FC) are alienated to produce a reference current for the hysteresis-band controller. Generally, the conventional system consists of SHAPF control and PLL. Where a PLL is used to split the positive sequenced components from the source voltage, in the suggested control method, STF is used. In addition, STF also does the work of LPFs and HPFs for splitting the FC of the current. Therefore, the proposed control consists of an STF, SHAPF, and SAPF.

3.1. Modelling of STF

Hong-Sock calculated the integral in the synchronous reference frame (SRF) given in Equation (15)

$$V_{xy}(t) = e^{j\omega t} \int e^{-j\omega t} U_{xy}(t) dt \tag{15}$$

where U_{xy} and V_{xy} are instantaneous signals in the SRF as former and later integration. The transfer function $H(s)$ is provided in Equation (16) by applying the Laplace transform to Equation (15).

$$H(s) = \frac{V_{xy}(s)}{U_{xy}(s)} = \frac{s + j\omega}{s^2 + \omega^2} \tag{16}$$

In order to get STF with a cut-off frequency from $H(s)$, a constant parameter k is introduced. Thus, $H(s)$ is given in Equation (17).

$$H(s) = \frac{V_{xy}(s)}{U_{xy}(s)} = \frac{k(s + k) + j\omega_n}{(s + k)^2 + \omega_n^2} \tag{17}$$

By swapping $U_{xy}(s)$ by $x_{\alpha\beta}(s)$ and $V_{xy}(s)$ by $x'_{\alpha\beta}(s)$, Equations (18) and (19) are obtained:

$$x'_{\alpha}(s) = \left(\frac{k}{s} [x_{\alpha}(s) - x'_{\alpha}(s)] - \frac{\omega_n}{s} .x'_{\beta}(s)\right) \tag{18}$$

$$x'_{\beta}(s) = \left(\frac{k}{s} [x_{\beta}(s) - x'_{\beta}(s)] - \frac{\omega_n}{s} .x'_{\alpha}(s)\right) \tag{19}$$

where ω_n is the expected frequency of output and k is the filter’s gain. If the value k increases the accuracy of extracting, the desired component increases and vice-versa. Therefore, by using an STF, distortional signals of both voltage and current can be acquired without any change in their magnitude and phase angle. The control structure of an STF is shown in Figure 5.

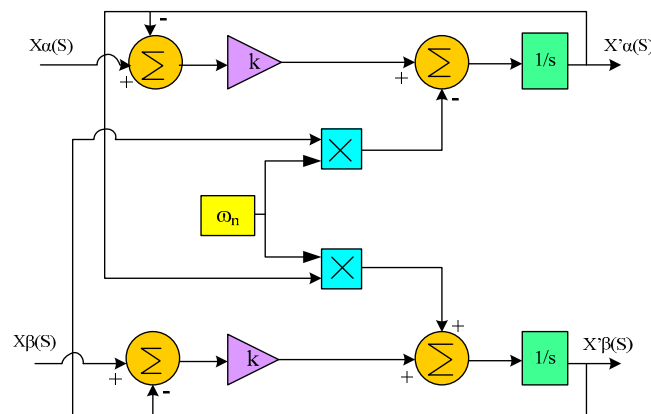


Figure 5. The control structure of STF.

3.2. SHAPF

The prime motive role of SHAPF is to reduce the THD of the supply current thereby improving the power factor (PF) by injecting the appropriate current. In addition, it maintains a constant voltage across the DC-Link. The proposed system (i) performs abc- $\alpha\beta$, $\alpha\beta$ -dq, dq- $\alpha\beta$, and $\alpha\beta$ -abc domain conversions; and (ii) NFIHC is used for regulating voltage across DC-Link capacitor and reducing harmonics in the current waveform. The NFIHC compares the actual DC capacitor voltage V_{dc} with V_{dc}^{ref} and injects the error into the axis. The schematic diagram of the NFIHC is given in Figure 6. STF is used to generate SYP and for the splitting of FC and HC of the current. The domain transformations of STF, the design, and control part of the NFIHC are given below:

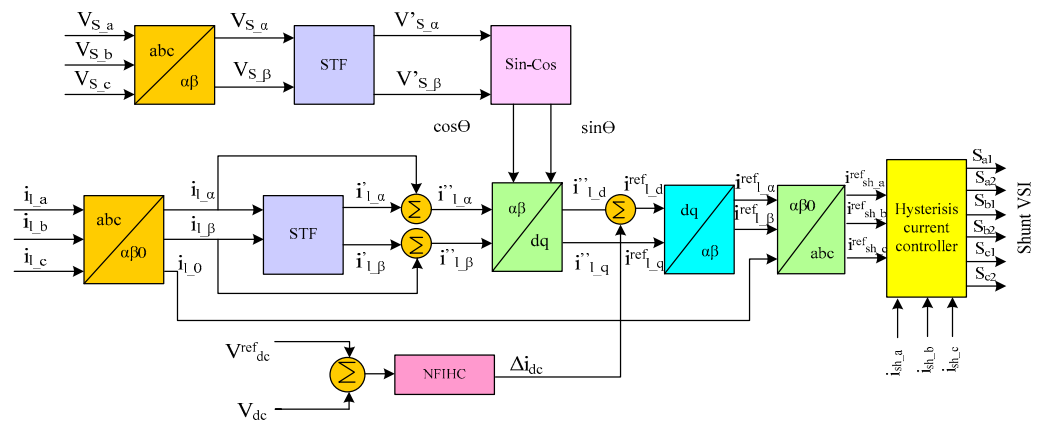


Figure 6. NFIHC for Shunt Converter.

The SHAPF is controlled by the d-q theory. According to it, load currents are transferred to α - β -0 coordinates using Clark’s transformation by Equation (20).

$$\begin{bmatrix} i_{l_\alpha} \\ i_{l_\beta} \\ i_{l_0} \end{bmatrix} = \sqrt{\frac{2}{3}} \begin{bmatrix} 1 & -\frac{1}{2} & -\frac{1}{2} \\ 0 & \frac{\sqrt{3}}{2} & -\frac{\sqrt{3}}{2} \\ \frac{1}{2} & \frac{1}{2} & \frac{1}{2} \end{bmatrix} \begin{bmatrix} i_{l_a} \\ i_{l_b} \\ i_{l_c} \end{bmatrix} \tag{20}$$

By the implementation of the Laplace transformation, the STF separates the HC from FC by using the Equation (21).

$$\begin{bmatrix} i'_{l_\alpha}(s) \\ i'_{l_\beta}(s) \end{bmatrix} = \frac{k_2}{s} \begin{bmatrix} i_{l_\alpha}(s) - i'_{l_\alpha}(s) \\ i_{l_\beta}(s) + i'_{l_\beta}(s) \end{bmatrix} + \frac{2\pi f_{c2}}{s} \begin{bmatrix} i_{l_\beta}(s) \\ -i_{l_\alpha}(s) \end{bmatrix} \tag{21}$$

Here k_2 is the constant gain whose value is chosen as 20 and f_{c2} is the cut-off frequency rating equal to system frequency 50 Hz. The HC in α - β -0 coordinates are obtained by Equation (22).

$$\begin{aligned} i''_{l_\alpha} &= i_{l_\alpha} - i'_{l_\alpha} \\ i''_{l_\beta} &= i_{l_\beta} - i'_{l_\beta} \end{aligned} \tag{22}$$

In Equation (23), the Clarke transformation is applied to transform the supply voltage from abc to α - β -0 domain.

$$\begin{bmatrix} V_{S_\alpha} \\ V_{S_\beta} \\ V_{S_0} \end{bmatrix} = \sqrt{\frac{2}{3}} \begin{bmatrix} 1 & -\frac{1}{2} & -\frac{1}{2} \\ 0 & \frac{\sqrt{3}}{2} & -\frac{\sqrt{3}}{2} \\ \frac{1}{2} & \frac{1}{2} & \frac{1}{2} \end{bmatrix} \begin{bmatrix} V_{S_a} \\ V_{S_b} \\ V_{S_c} \end{bmatrix} \tag{23}$$

The SYP $\sin(\omega t)$ and $\cos(\omega t)$ are obtained from Equation (24), which eliminates conventional PLL.

$$\begin{bmatrix} \sin(\omega t) \\ \cos(\omega t) \end{bmatrix} = \frac{1}{\sqrt{(V_{S_\alpha})^2 + (V_{S_\beta})^2}} \begin{bmatrix} V_{S_\alpha} \\ -V_{S_\beta} \end{bmatrix} \tag{24}$$

The HC obtained in Equation (22) and the SYP obtained from Equation (24) are used to obtain HC in the d-frame.

$$i''_{l_d} = i''_{l_\alpha} \sin(\omega t) - i''_{l_\alpha} \cos(\omega t) \tag{25}$$

The performance of SHAPF depends on both the reference current generation and DC-Link voltage. Therefore, it is important to maintain a constant DC-Link voltage. Whenever the load varies, the active power flow in the SHAPF varies, which in turn varies the DC-Link voltage. Therefore, to maintain the constant DC-Link voltage, the active power in SHAPF must be regulated. To achieve it, the active power flow in the SHAPF was made equal to the switching loss of the filter. The proposed NFIHC injects a suitable error signal Δi_{dc} in the d axis from the difference between the actual and reference DC-Link voltages. Therefore, the proper selection and design of the controller play a key role in DC-Link voltage regulation. The grid reference current in the d-axis is given by Equation (26).

$$i^{ref}_{l_d} = i''_{l_d} - \Delta i_{dc} \tag{26}$$

The reference d - q load currents are converted into α - β domain by using Equation (27). Next, the shunt injected reference currents in abc the domain are obtained from Equation (28).

$$\begin{bmatrix} i^{ref}_{l_\alpha} \\ i^{ref}_{l_\beta} \end{bmatrix} = \begin{bmatrix} \sin(\omega t) & \cos(\omega t) \\ -\cos(\omega t) & \sin(\omega t) \end{bmatrix} \begin{bmatrix} i^{ref}_{l_d} \\ i^{ref}_{l_q} \end{bmatrix} \tag{27}$$

$$\begin{bmatrix} i^{ref}_{sh_a} \\ i^{ref}_{sh_b} \\ i^{ref}_{sh_c} \end{bmatrix} = \sqrt{\frac{2}{3}} \begin{bmatrix} 1 & 0 \\ -\frac{1}{2} & \frac{\sqrt{3}}{2} \\ -\frac{1}{2} & -\frac{\sqrt{3}}{2} \end{bmatrix} \begin{bmatrix} i^{ref}_{l_\alpha} \\ i^{ref}_{l_\beta} \end{bmatrix} \tag{28}$$

The errors obtained from the comparison of the measured currents with these reference currents are supplied to a hysteresis controller to generate shunt converter switching signals.

Proposed NFIHC

The NFIHC is an amalgamation of FL and ANN techniques, where the process of FL is controlled by the ANN technique. The FL controller works on mathematical reasoning, i.e., on linguistic rules. The FL controller works in three stages: fuzzification, inference, and defuzzification. During the processes of fuzzification, the numerical inputs are converted into linguistic variables. In order to transform the values into linguistic terms, a set of MFs is developed. The fuzzy rule base and MFs are determined in the inference stage. Lastly, in the stage of defuzzification depending on the input, any one of the values is considered as output. The process of FL is given in Figure 7.

The Takagi–Sugeno method is considered and receives Er and CE as inputs. The E is evaluated by Equation (29). The triangle MFs for both the E and CE are shown in Figures 8 and 9, respectively. The fuzzy variables are denoted by triangular MFs as given in Figures 8 and 9, involving P1, medium positive (P2), P0, Zero (O), N2, medium negative (N1), and N0. The voltage across DC-Link considers values in the range of these linguistic terms, and it is operated in a total of 49 sets of MFs, as exhibited in Table 4.

$$E_r = V^{ref}_{dc} - V^i_{dc}; \quad i = 1, 2, 3, 4, 5, 6 \tag{29}$$

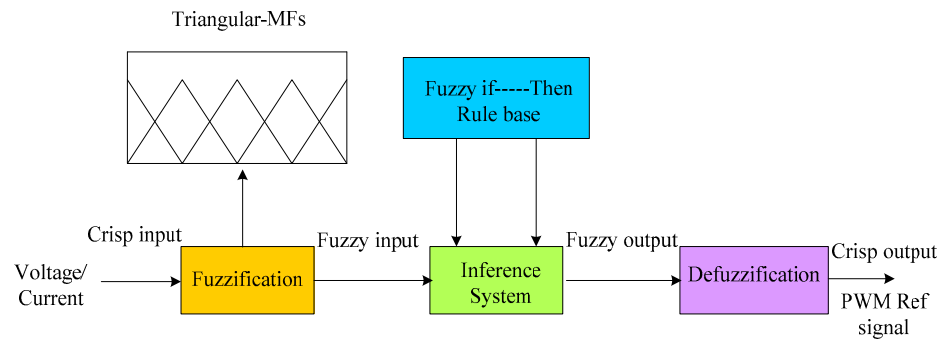


Figure 7. Overview of Fuzzy controller.

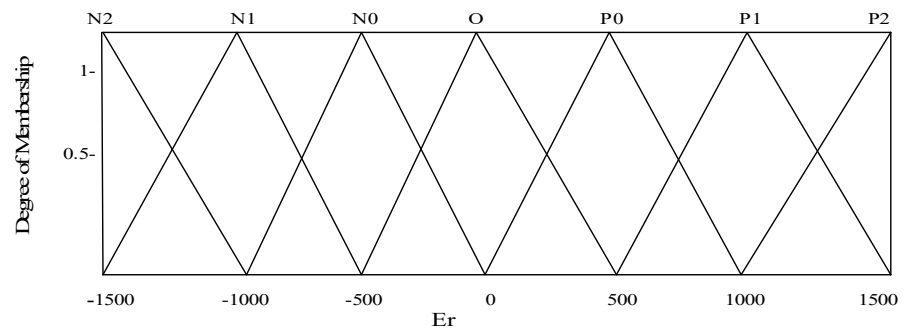


Figure 8. MF for “Er”.

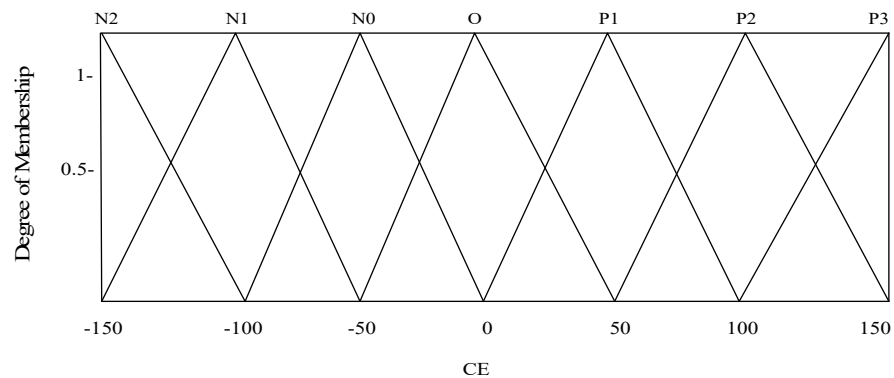


Figure 9. MF for “CE”.

Table 4. MF mapping for capacitor voltage.

Er	CE						
	P2	P1	P0	O	N0	N1	N2
N2	O	N0	N1	N2	N2	N2	N2
N1	P0	O	N0	N1	N2	N2	N2
N0	P1	P0	O	N0	N1	N2	N2
O	P2	P1	P0	O	N0	N1	N2
P0	P2	P2	P1	P0	O	N0	N1
P1	P2	P2	P2	P1	P0	O	N0
P2	P2	P2	P2	P2	P1	P0	O

The ANN is a self-adaptive advanced control technique; its working mechanism is similar to the human brain. It is preferable due to its self-training, where interconnected neurons are trained according to the task required. The ANN contains three layers, namely IPL to receive data, HDL (between IPL and OPL), possessing specific weights and bias, and OPL, providing the output.

The proposed NFIHC is an efficient self-adaptive controller that utilizes both the superior qualities of FL and ANN controllers. Initially, the given inputs are trained by the MFs of FL and fed as inputs to the ANN. Based on the number of HDL, the NFIHC trains and provides appropriate output. The schematic diagram of NFIHC is illustrated in Figure 10. The MFs are trained through the NFIHC method to produce the desired output. In the proposed WPGS, and BSS connected SHAPF, the reference DC voltage is compared with the actual voltage, and the error is fed to the NFIHC controller. In this paper, the Levenberg–Marquardt algorithm is used to train the ANN.

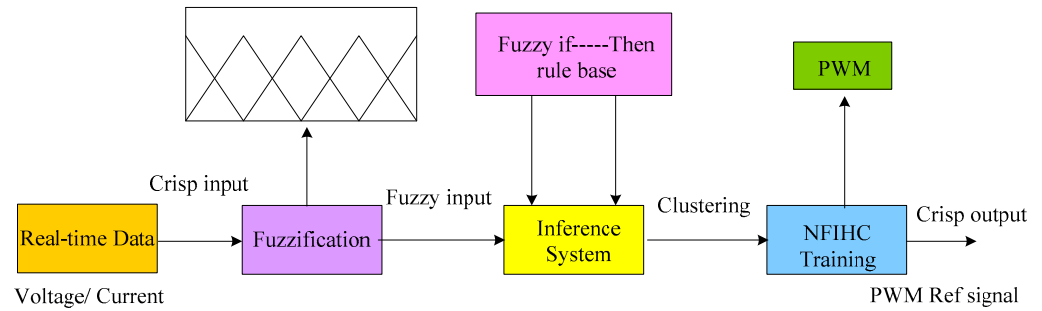


Figure 10. Overview of NFIHC.

The NFIHC system is mathematically modeled by Equation (30).

$$\text{IF } M \text{ is } G \text{ AND } N \text{ is } H, \text{ then } P = F(M, N) \tag{30}$$

where

$M, N,$ and P are input and output parameters.

A total of five layers were considered. At the 1st, the MFs with input M are represented as $\delta_{G_j}(M)$, where j denotes the MFs used. The weight (W) of neurons (i) at the product layer with AND operator is given in Equation (31).

$$W_i = \delta_{G_j}(M) * \delta_{H_j}(N) \tag{31}$$

The 3rd layer works for the normalization of the values received from the 2nd layer and are expressed in Equation (32).

$$W_i = \frac{W_i}{W_1 + W_2} \tag{32}$$

In the 4th defuzzification layer, the ANN controller adopts self-adaptive property with the inference parameters (a_i, b_i, c_i) as given in Equation (33).

$$\overline{W}_i F_i = \overline{W}_i (a_i M + b_i N + c_i) \tag{33}$$

The summation of inputs is carried out at the 5th layer to produce the output function F as given in Equation (34).

$$F = \sum_i \overline{W}_i F_i \tag{34}$$

The block diagram showing the five layers of the proposed NFIHC is given in Figure 11. The fuzzy rules that are applied are given in Equations (35) and (36). The flow chart of the proposed method is given in the Figure 12.

$$\text{If } M \text{ is } G_1 \text{ AND } N \text{ is } H_1, \text{ then } F_1 = a_1 M + b_1 N + c_1 \tag{35}$$

$$\text{If } M \text{ is } G_2 \text{ AND } N \text{ is } H_2, \text{ then } F_2 = a_2 M + b_2 N + c_2 \tag{36}$$

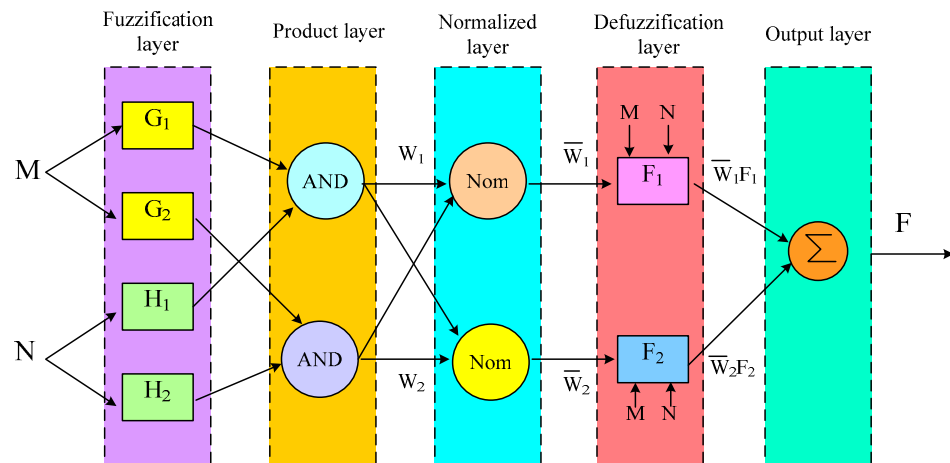


Figure 11. Structure of NFIHC.

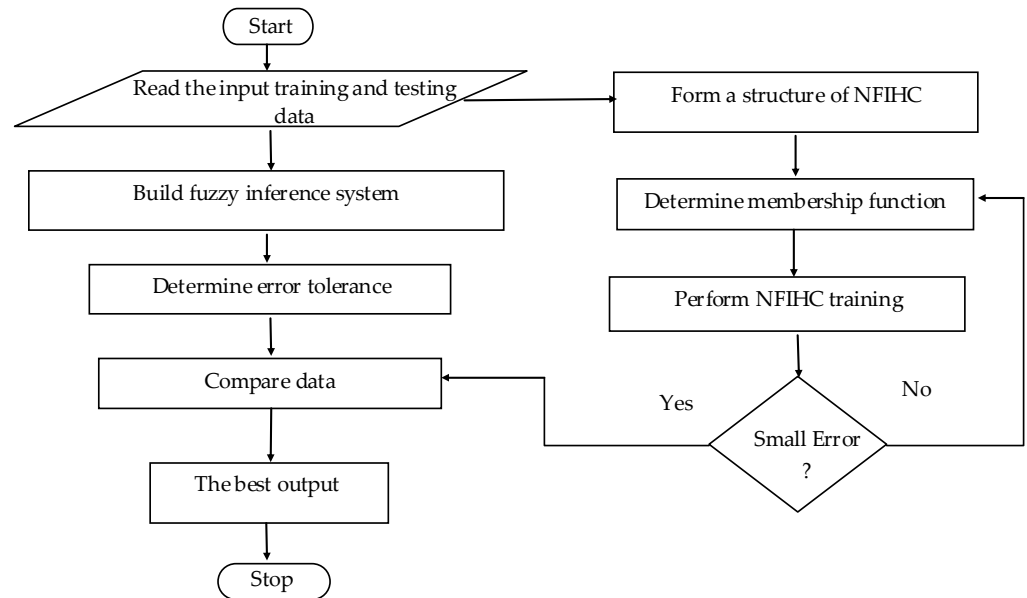


Figure 12. Flow of the proposed method.

4. Simulation Results and Discussion

A 3-phase AC distribution network was explored to study the efficiency of the suggested SH-SPVBS. Five cases with different combinations of balanced/unbalanced non-linear loads and balanced/unbalanced supply voltages were considered to prove the superior performance of the proposed system as given in Table 5. The supply voltage is considered to be balanced for cases 1–4 and unbalanced for case5. The obtained THD & PF of the supply current for the proposed NFIHC method is compared with those of existing techniques such as PI, ANN, and FL controllers and other controllers that are available in the literature for validation as given in Figures 13 and 14 and Table 6, respectively. The PF is calculated by Equation (37).

$$PF = \cos \theta * \frac{1}{\sqrt{1 + THD^2}} \tag{37}$$

where θ is the angle between voltage and current, with $\frac{1}{\sqrt{1+THD^2}}$ representing the displacement factor.

Table 5. Case studies considered.

Load	Case 1	Case 2	Case 3	Case 4	Case 5
Balanced supply voltage	✓	✓	✓	✓	
Unbalanced supply voltage					✓
11 m/s wind speed	✓	✓		✓	
10 m/s wind speed			✓		✓
Balanced Rectifier Load: 30.00 Ω & 20.00 mH	✓		✓	✓	
Unbalanced R-L Load: R: 10, 20 & 15 Ω; L: 9.50, 10.50 & 18.50 mH.		✓		✓	✓
Induction Furnace load: LC = 400.0 mH, 50.0 μF RL = 10.0 Ω, 100.0 mH			✓		

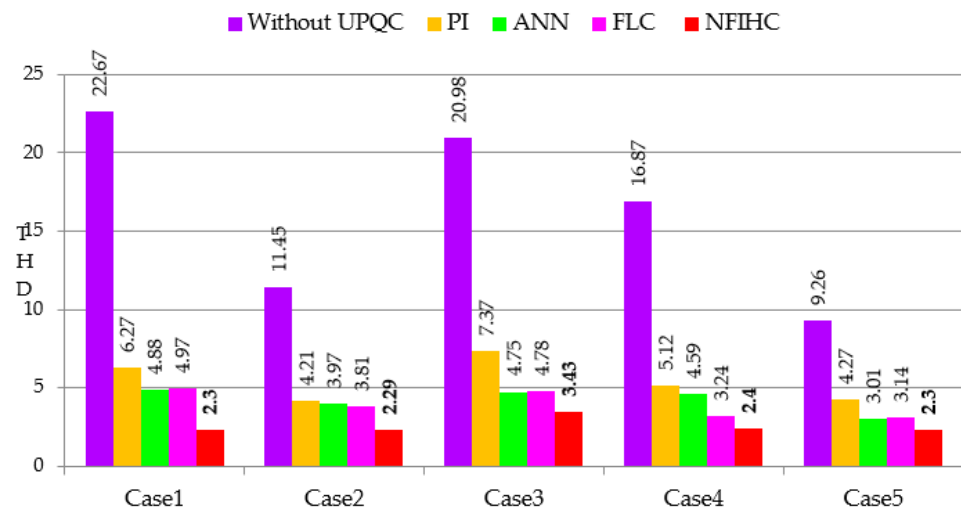


Figure 13. THD comparison of the proposed method with the controllers considered in the study.

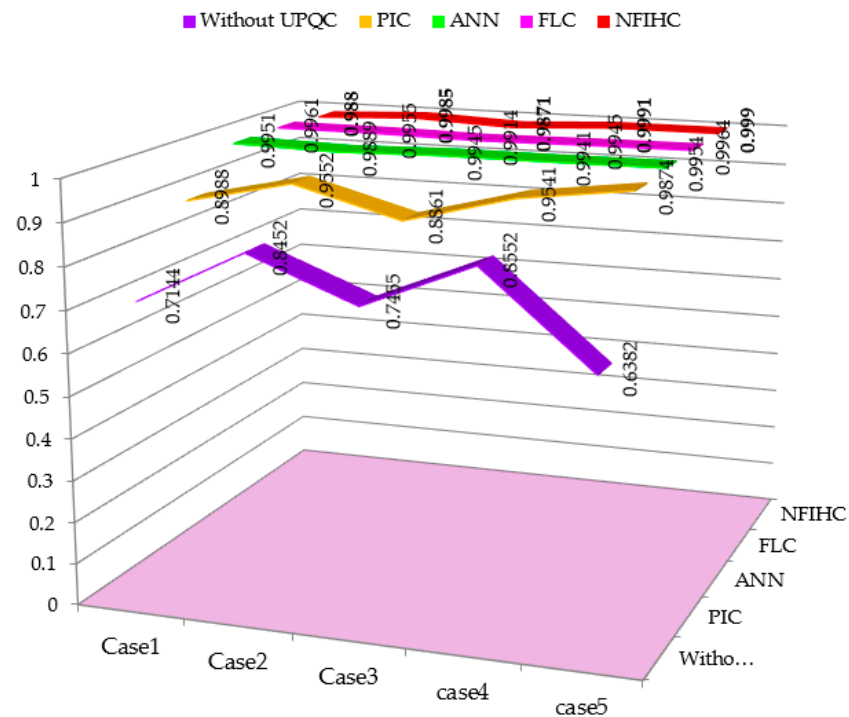


Figure 14. PF comparison.

Table 6. % THD comparison of proposed controller with controllers that are available in the literature.

Method	Case 1	Case 2	Case 3	Case 4	Case 5
Without SH-SPVBS	22.67	11.45	20.98	16.87	9.26
PI	6.27	4.21	4.37	5.12	4.27
ANN	4.88	3.97	4.75	4.59	3.01
FL	4.97	3.81	4.78	3.24	3.14
PI-C [20]	3.28	–	–	–	–
SMC [20]	2.44	–	–	–	–
PI [25]	14.74	–	–	–	–
FL [25]	6.13	–	–	–	–
ANFIS [25]	2.43	–	–	–	–
PIC [33]	3.65	–	–	–	–
FLC [33]	2.52	–	–	–	–
NFIHC	2.30	2.29	3.43	2.4	2.30

The waveforms during steady-state conditions of the proposed SH-WPBS test system for all cases 1–5 are shown in Figures 15–19.

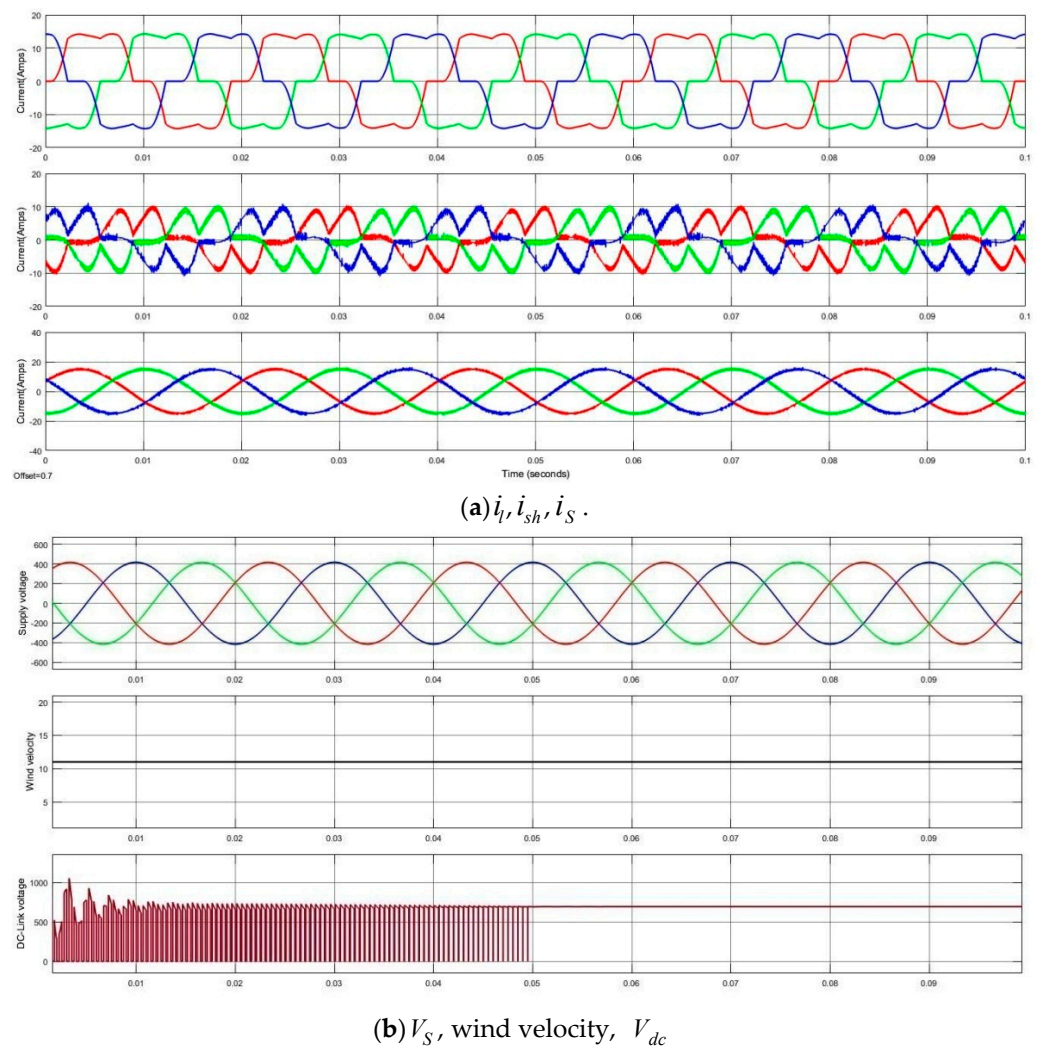
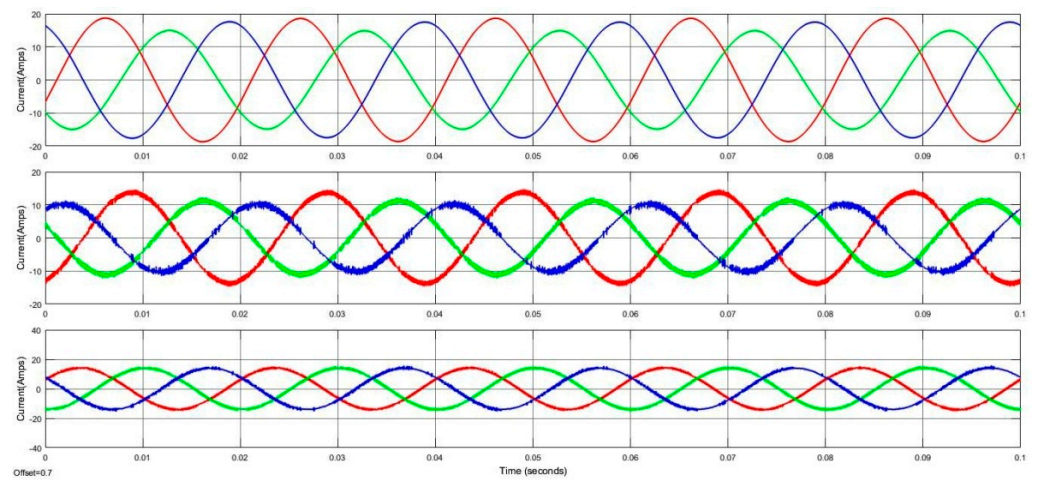
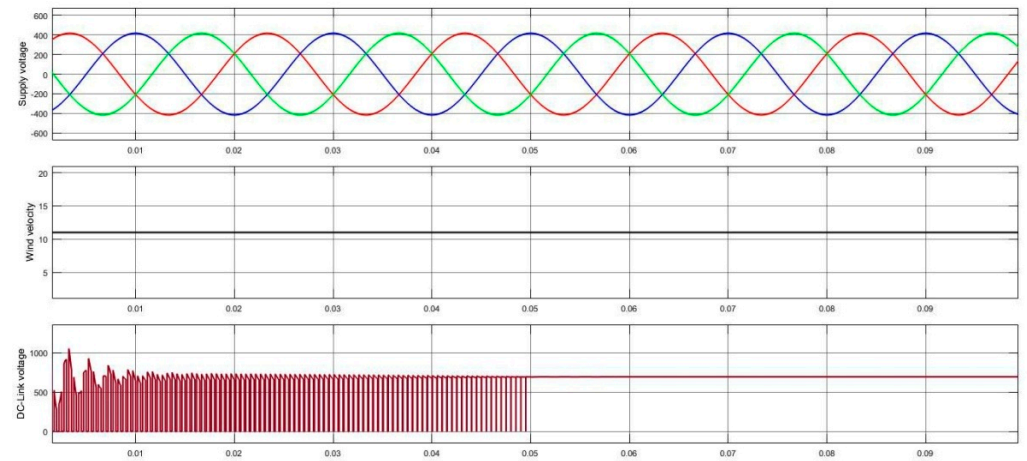


Figure 15. Waveforms for case 1.

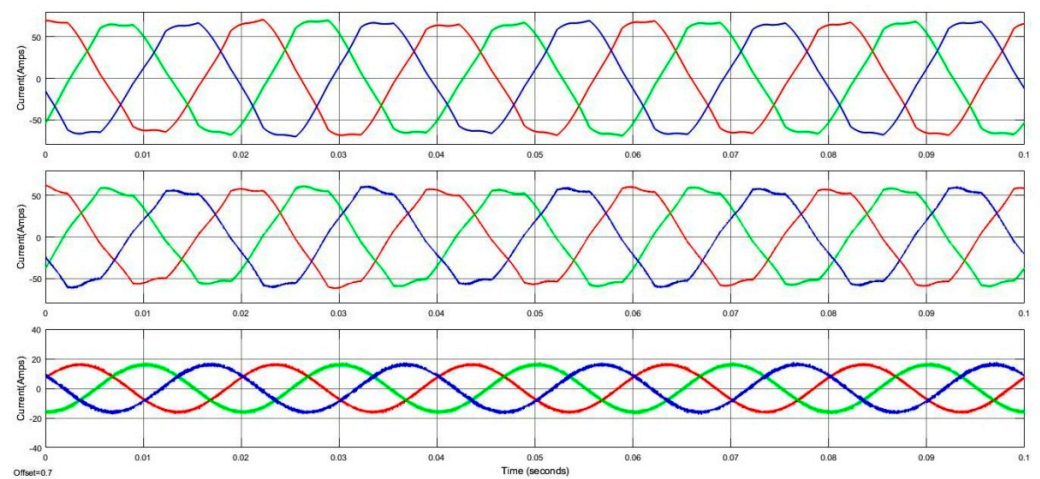


(a) i_r, i_{sh}, i_S .



(b) V_S , wind velocity, V_{dc}

Figure 16. Waveforms for case 2.



(a) i_r, i_{sh}, i_S .

Figure 17. Cont.

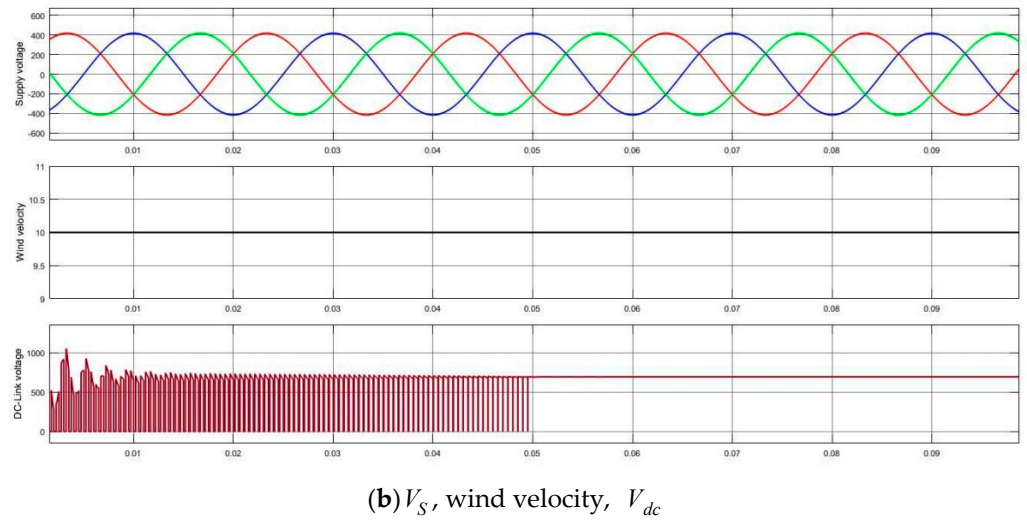


Figure 17. Waveforms for case 3.

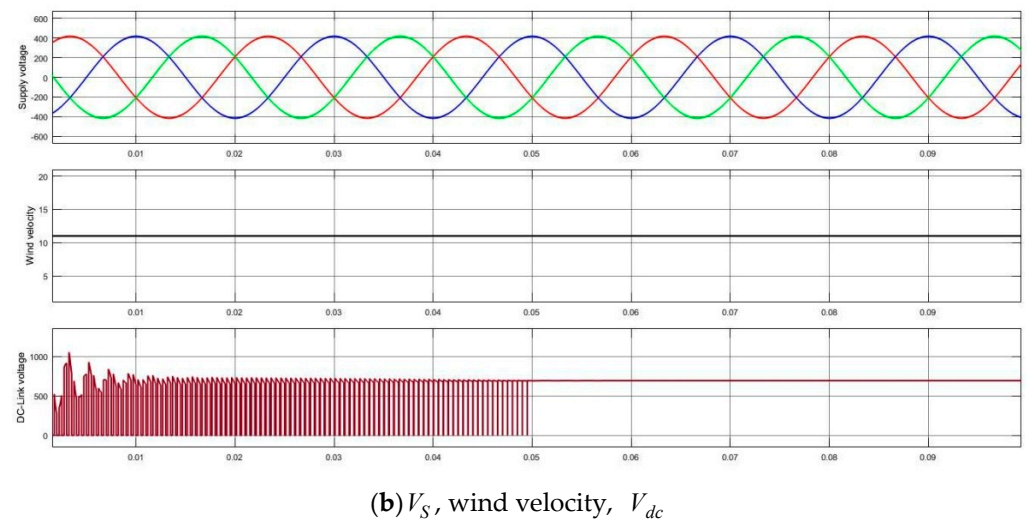
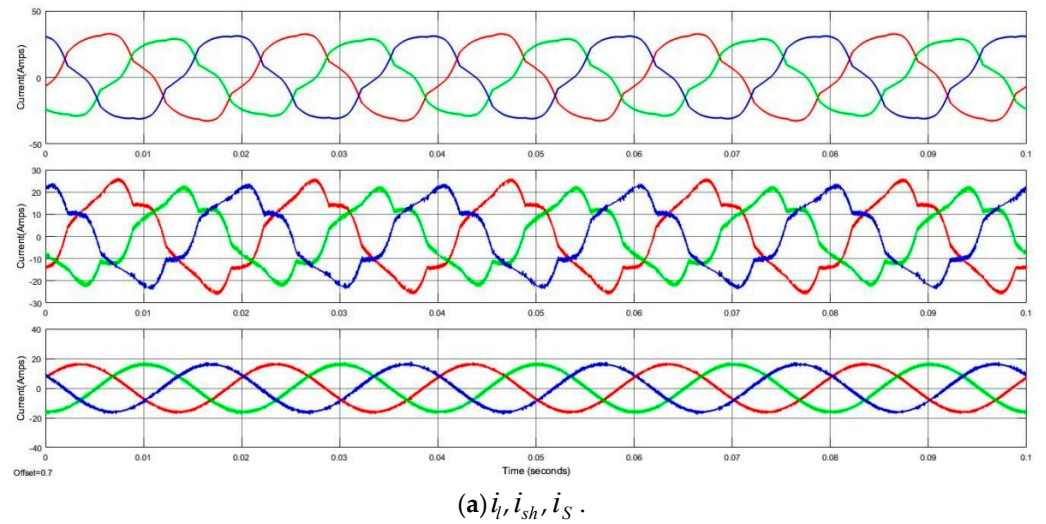


Figure 18. Waveforms for case 4.

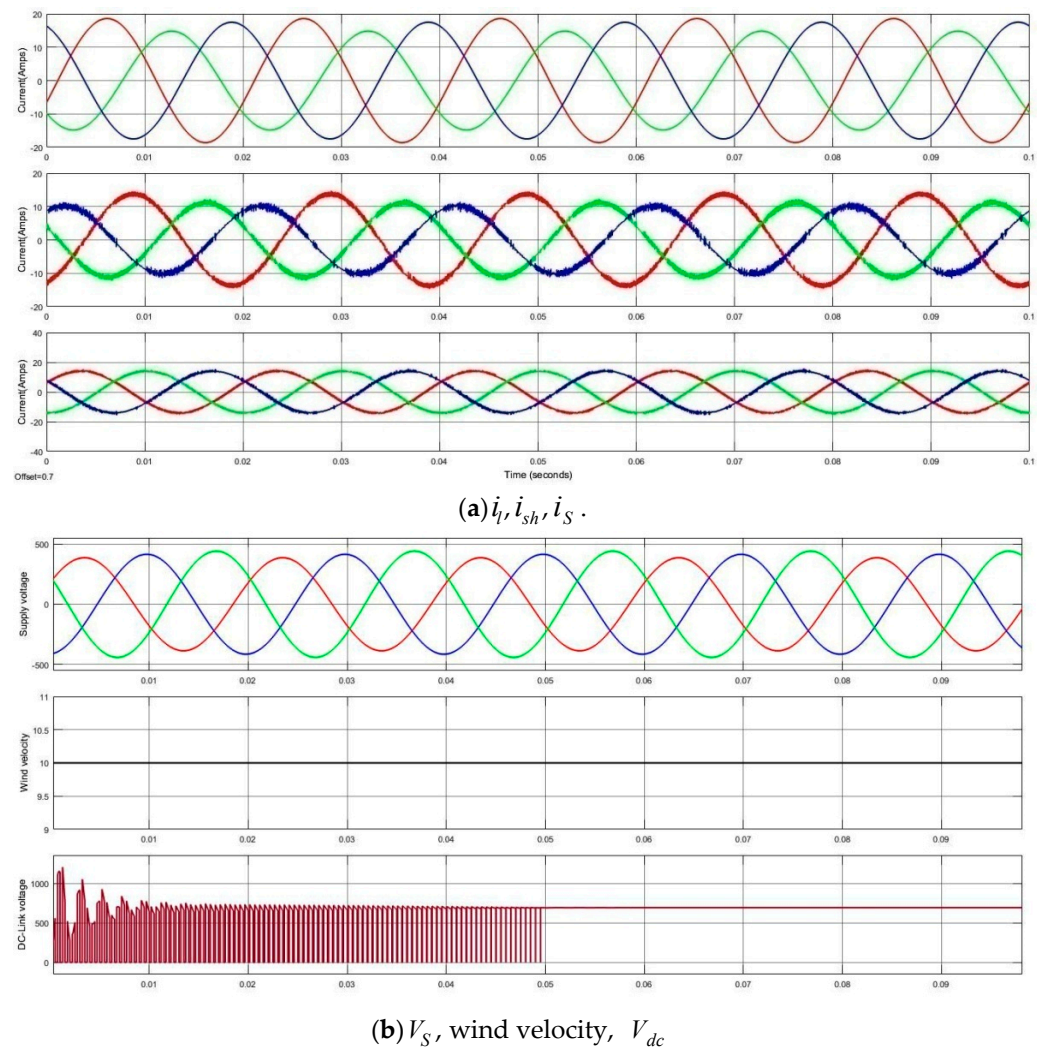


Figure 19. Waveforms for case 5.

In case 1, the source voltage was considered to be balanced for a three-phase balanced rectifier load with a constant 11 m/s wind velocity. The load currents were observed to be balanced but non-sinusoidal due to the nonlinear load. It is observed clearly from Figure 15a that the proposed method can give a sinusoidal source current. Such improvement in the waveforms has an impact on the THD and PF values. By injecting suitable shunt currents, the current's THD was decreased from 22.67 percent to 2.30 percent, which is lower than that of methods available in the literature given in Table 6, and the PF was raised from 0.714 to 0.988. In addition, the DC-Link voltage was maintained constant with a low settling time of 0.05 s as shown in Figure 15b.

In case 2, the balanced supply voltage for the unbalanced load with 11 m/s wind velocity was considered; the load current was sinusoidal and unbalanced as presented in Figure 16a. It can be observed clearly that the NFIHC was able to reduce the THD from 11.45% to 2.29% effectively. As a result, the PF value boosted from 0.8452 to 0.9985. However, as shown in Figure 16b, the DC-link voltage was maintained constant during load change.

In case 3, the load current was non-sinusoidal and balanced due to the rectifier and furnace combined load as shown in Figure 17a. By injecting the required currents, the NFIHC can reduce THD from 20.98 percent to 3.43 percent and enhance PF from 0.7455 to 0.9871 percent. In addition, it proves that it maintains a constant DC-Link voltage during load and wind speed variation from 11 m/s to 10 m/s as illustrated in Figure 17b.

In case 4, due to the combination of both nonlinear balanced and unbalanced loads being considered, the load current was non-sinusoidal and unbalanced as presented in Figure 18a. It can be clearly observed that the NFIHC was able to reduce the THD from 16.87% to 2.4% effectively. As a result, the PF value rose from 0.8552 to 0.991.

In case 5, due to the unbalanced supply and unbalanced load with a wind speed of 10m/s, the load current was sinusoidal and unbalanced, as shown in Figure 19a with a THD of 9.26% and PF of 0.6382. The proposed hybrid controller effectively reduces THD from 9.26% to 2.30% and boosts PF from 0.6382 to 0.999. The proposed method was also able to maintain voltage across the DC-link effectively during the wind velocity variation, as shown in Figure 19b. The THD comparison for all the test cases is given in Figure 13. However, from Figure 14, it is clearly observed that the proposed method boosts up the PF to a much higher value almost to unity when compared to other control techniques for all the test studies efficiently. From the waveforms 15–29, it is clearly observed that the time required to reach the stable DC-link voltage without peak overshoot is 0.05sec, which is much less than conventional methods. Figure 20 exhibits the superior performance of the proposed method in maintaining constant DC-Link voltage during wind velocity variations. Figure 21 gives the THD spectrum of the proposed method for all the test cases for validation.

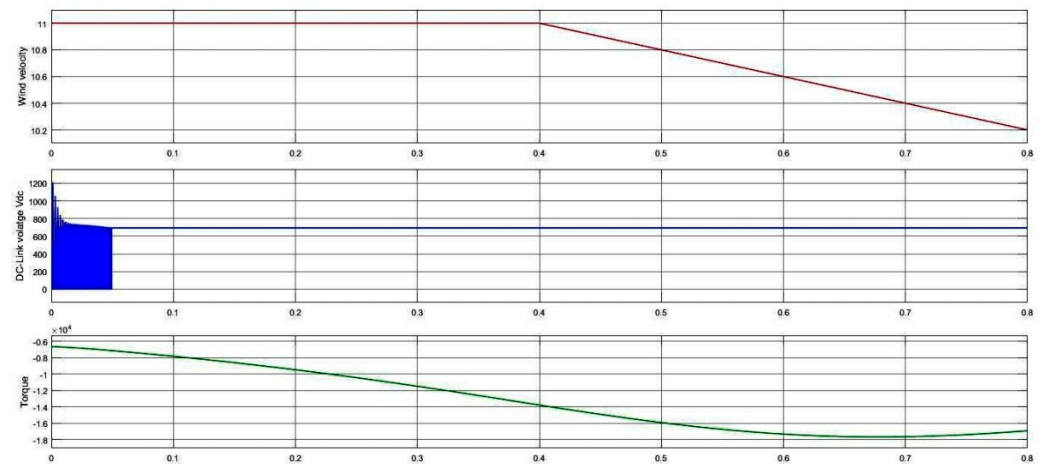
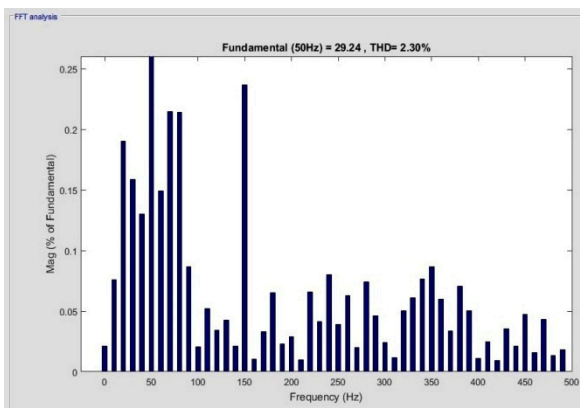
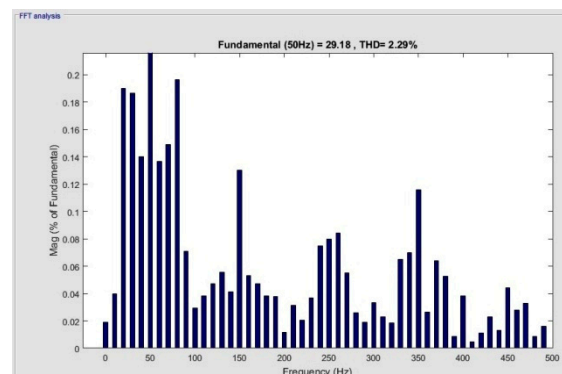


Figure 20. Waveforms for wind velocity variation, DC-Link voltage, torque.



(a) Case-1



(b) Case-2

Figure 21. Cont.

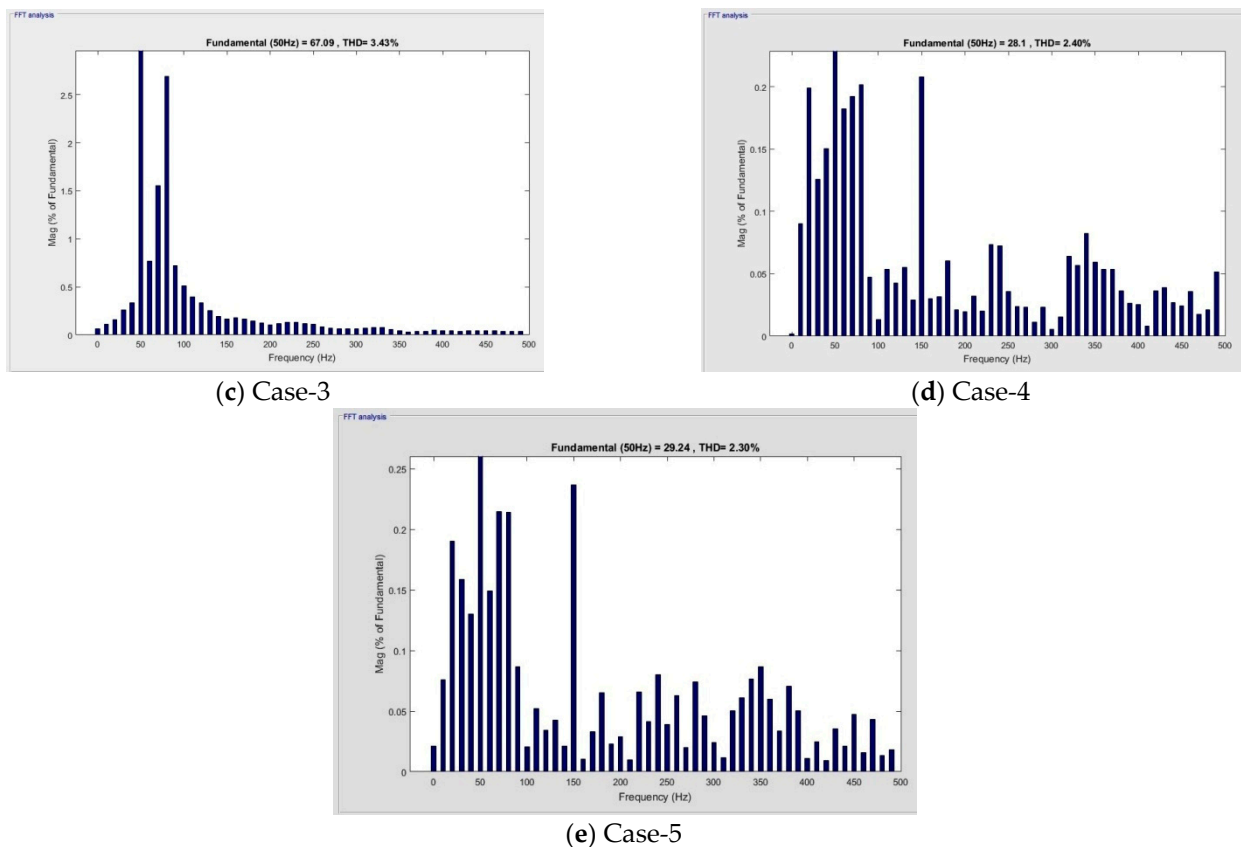


Figure 21. THD spectrum.

5. Conclusions

A hybrid NFIHC combination of both the properties of FL and ANN controllers was proposed for STF-based SH-WPBS. STF is used to produce SYP for SH-WPBS avoiding conventional PLL in addition to the splitting of FC and HC of currents. The STF with transformations was also given in addition to the design of NFIHC. The proposed method was able to lower THDs within acceptable values, boost PF to almost unity, and maintain stable DC-Link voltage after studying five test scenarios with diverse load combinations, and balanced and unbalanced source voltages. Moreover, these performances were much better than those of the existing controllers of PI, FL, and ANN. The NFIHC also maintains a constant DC-link voltage for all variations in wind velocity. To validate the proposed method, the obtained %THD was compared with those of the latest methods that are available in the literature. As a part of future research, the proposed model might be tested on an island condition. In addition, the hybrid controller technique can also be implemented in the series active power filter.

Author Contributions: Conceptualization, S.K. and K.J.K.; methodology, S.R.S.; software, S.K.; validation, S.K., K.J.K., and S.R.S.; formal analysis, S.K.; investigation, K.J.K.; resources, S.R.S.; data curation, S.K.; writing—original draft preparation, K.J.K.; writing—review and editing, S.K., K.J.K., and S.R.S.; visualization, S.K.; supervision, K.J.K. and S.R.S.; project administration, S.K.; funding acquisition, S.K., K.J.K., and S.R.S. All authors have read and agreed to the published version of the manuscript.

Funding: This research was funded by “Woosong University’s Academic Research Funding—2022”.

Institutional Review Board Statement: Not Applicable.

Informed Consent Statement: Not Applicable.

Data Availability Statement: Not applicable.

Conflicts of Interest: The authors declare no conflict of interest.

Nomenclature

$V_{S_a}, V_{S_b}, V_{S_c}$	Source voltage for phases a, b, c
$V_{S_\alpha}, V_{S_\beta}, V_{S_0}$	Source voltage in α - β -0 domain
$V'_{S_\alpha}, V'_{S_\beta}, V'_{S_0}$	FC of source voltage in α - β -0 domain
$i_{S_a}, i_{S_b}, i_{S_c}$	Source current for phases a, b, c
R_S	Source Resistance
L_S	Source Inductance
$V_{L_a}, V_{L_b}, V_{L_c}$	Load voltage for phases a, b, c
$i_{L_a}, i_{L_b}, i_{L_c}$	Load current for phases a, b, c
$i_{L_\alpha}, i_{L_\beta}, i_{L_0}$	Load currents in α - β -0 domain
$i'_{L_\alpha}, i'_{L_\beta}, i'_{L_0}$	FC of load currents in α - β -0 domain
$i''_{L_\alpha}, i''_{L_\beta}, i''_{L_0}$	HC of load currents in α - β -0 domain
i''_{L_d}, i''_{L_q}	HC of load currents in d - q domain
$i^{ref}_{L_a}, i^{ref}_{L_b}, i^{ref}_{L_c}$	Reference load current for phases abc
$i^{ref}_{L_\alpha}, i^{ref}_{L_\beta}, i^{ref}_{L_0}$	Reference load current α - β -0 domain
$i^{ref}_{L_d}, i^{ref}_{L_q}$	Reference load current in d - q domain
$i_{sh_a}, i_{sh_b}, i_{sh_c}$	SHAPF-injected current for phases a, b, c
$i^{ref}_{sh_a}, i^{ref}_{sh_b}, i^{ref}_{sh_c}$	Reference SHAPF injected current for phases abc
C_{sh}	Capacitance of SHAPF
R_{sh}	Resistance of SHAPF
L_{sh}	Inductance of SHAPF
C_{dc}	DC-Link capacitance
V_{dc}	Actual DC-Link capacitor voltage
V^{ref}_{dc}	DC-Link reference voltage
Δi_{dc}	Dc link error
P_W	Wind output power
V_W	Wind output voltage
i_W	Wind output current
P_{dc}	Power demand at DC-Link
Q	Battery rated capacity
V_{BS}	Battery output voltage
i_{BS}	Battery output current
DPD	DC-Link power demand
MFs	Membership Functions
IPL	Input-layer
HDL	Hidden-layer
OPL	Output-layer
SOC	state-of-charge
E_r	Error
CE	Change in error
SRFT	Synchronous Reference-frame theory
TSR	Tip speed Ratio
HCC	Hysteresis current control

References

- Vijayakumar, G.; Nitin, G.; Gupta, R.A. Mitigation of power quality problems using shunt active power filters: A comprehensive review. In Proceedings of the 12th IEEE Conference on Industrial Electronics and Applications (ICIEA), Siem Reap, Cambodia, 18–20 June 2017.
- Metin, K.; Engin, O. Synchronous-Reference-Frame-Based Control Method for UPQC under Unbalanced and Distorted Load Conditions. *IEEE Trans. Ind. Electron.* **2011**, *58*, 3967–3975.
- Suresh, M.; Panda, A.K. PI and Fuzzy Logic Controller based 3-phase 4-wire Shunt active filter for mitigation of Current harmonics with Id-Iq Control Strategy. *J. Power Electron.* **2011**, *11*, 914–921.
- Soumya, R.D.; Prakash, K.R.; Asit, M.; Gayadhar, P. Power Quality Enhancement in PV and Battery Storage Based Microgrid Using Hybrid Active Filter. In Proceedings of the 3rd International Conference on Energy, Power and Environment: Towards Clean Energy Technologies, Shillong, India, 5–7 March 2021.
- Suresh, M.; Panda, A.K. RTDS hardware implementation and simulation of SHAF for mitigation of harmonics using p-q control strategy with PI and Fuzzy logic controllers. *Front. Electr. Electron. Eng.* **2012**, *7*, 427–437.

6. Lin, H.C. Intelligent Neural Network-Based Fast Power System Harmonic Detection. *IEEE Trans. Ind. Electron.* **2007**, *54*, 43–52. [[CrossRef](#)]
7. Dash, P.K.; Panda, S.K.; Lee, T.H.; Xu, J.U.; Routray, A. Fuzzy and Neural Controllers for Dynamic Systems: An Overview. In Proceedings of the Second International Conference on Power Electronics and Drive Systems, Singapore, 26–29 May 1997.
8. Sachin, D.; Bhim, S. Design and Performance Analysis of Three-Phase Solar PV Integrated UPQC. In Proceedings of the IEEE 6th International Conference on Power Systems(ICPS), New Delhi, India, 4–6 March 2016.
9. Viswanth, K.; Santanu, K.D.; Kumari, R.G. Development and Analysis of Power Quality by using Fuel cell based Shunt Active Power Filter. In Proceedings of the 2020 2nd International Conference on Innovative Mechanisms for Industry Applications (ICIMIA), Bangalore, India, 5–7 March 2020.
10. Alok, K.M.; Soumya, R.D.; Prakash, K.R.; Ranjan, K.M.; Asit, M.; Dillip, K.M. PSO-GWO Optimized Fractional Order PID Based Hybrid Shunt Active Power Filter for Power Quality Improvements. *IEEE Access* **2022**, *8*, 74497–74512.
11. Kumar, C.; Jaisiva, S.; Clement, R.A.; Logeshwari, V. Hybrid renewable energy based smart grid system for reactive power management and voltage profile enhancement using artificial neural network. *Energy Sources Part A Recovery Util. Environ. Eff.* **2021**, *43*, 2419–2442.
12. Mohanraj, M.R.; Prakash, R.A. Unified Power Quality Conditioner for Power Quality Improvement in Distributed Generation Network Using Adaptive Distributed Power Balanced Control (ADPBC). *Int. J. Wavelets Multi-Resolut. Inf. Process.* **2020**, *18*, 1941021. [[CrossRef](#)]
13. Krishna, S.; Debashis, C.; Goswami, S.K. A modified PV-wind-PEMFCS-based hybrid UPQC system with combined DVR/STATCOM operation by harmonic compensation. *Int. J. Model. Simul.* **2020**, *41*, 243–255.
14. Ramesh, J.; Suneel, T.; Prakash, R.B.; Vijay Muni, T. Analysis of sliding mode controller based DSTATCOM for power quality improvement in distribution power system. *Mater. Today Proc.* **2021**, in press.
15. Dheeban, S.S.; Muthu Selvan, N.B. ANFIS-based Power Quality Improvement by Photovoltaic Integrated UPQC at Distribution System. *IETE J. Res.* **2021**. [[CrossRef](#)]
16. Mohamed, A.; Philippe, P.; Shahram, K.; Shahrokh, S. New digital reference current generation for shunt active power filter under distorted voltage conditions. *Electr. Power Syst. Res.* **2009**, *79*, 759–765.
17. Almelian, M.; Mohd, I.; Omran, M.; Sheikh, U. Performance of unified power quality conditioner (UPQC) based on fuzzy controller for attenuating of voltage and current harmonics. *IOP Conf. Ser. Mater. Sci. Eng.* **2018**, *3*, 12–84. [[CrossRef](#)]
18. Vinothkumar, V.; Kanimozhi, R. Power flow control and power quality analysis in power distribution system using UPQC based cascaded multi-level inverter with predictive phase dispersion modulation method. *J. Ambient. Intell. Humaniz. Comput.* **2021**, *12*, 6445–6463. [[CrossRef](#)]
19. Tejinder, S.S.; Lakhwinder, S.; Gill, B.; Om Parkash, M. Effectiveness of UPQC in Mitigating Harmonics Generated by an Induction Furnace. *Electr. Power Compon. Syst.* **2018**, *46*, 629–636.
20. Samal, S.; Hota, P.K. Design and analysis of solar PV-fuel cell and wind energy based microgrid system for power quality improvement. *Cogent Eng.* **2017**, *4*, 1402453. [[CrossRef](#)]
21. Nandhini, E.; Sivaprakasam, A.A. Review of Various Control Strategies Based on Space Vector Pulse Width Modulation for the Voltage Source Inverter. *IETE J. Res.* **2020**, in press. [[CrossRef](#)]
22. Garima, G.; Pankaj, K.G. Self-adaptive learning based controller to mitigate PQ issues in internet of things devices. *Int. Trans. Electr. Energy Syst.* **2021**, *31*, e12888.
23. Nafeh, A.A.; Heikal, A.; El-Sehiemy, R.A.; Salem, W.A. Intelligent fuzzy-based controllers for voltage stability enhancement of AC-DC micro-grid with D-STATCOM. *Alex. Eng. J.* **2022**, *61*, 2260–2293.
24. Sayed, J.A.; Sabha, R.A.; Ranjan, K.J. Biogeography based optimization strategy for UPQC PI tuning on full order adaptive observer based control. *IET Gener. Transm. Distrib.* **2021**, *15*, 279–293.
25. Renduchintala, U.K.; Pang, C.; Tatikonda, K.M.; Yang, L. ANFIS-fuzzy logic based UPQC in interconnected microgrid distribution systems: Modeling, simulation and implementation. *J. Eng.* **2021**, *21*, 6–18. [[CrossRef](#)]
26. Devassy, S.; Singh, B. Performance analysis of solar pv array and battery integrated unified power quality conditioner for microgrid systems. *IEEE Trans. Ind. Electron.* **2021**, *68*, 4027–4035. [[CrossRef](#)]
27. Rajesh, P.; Shajin, F.H.; Umasankar, L. A Novel Control Scheme for PV/WT/FC/Battery to Power Quality Enhancement in Micro Grid System: A Hybrid Technique. *Energy Sources Part A Recovery Util. Environ. Eff.* **2021**, 1–17. [[CrossRef](#)]
28. Dheeban, S.S.; Muthu Selvan, N.B.; Umashankar, S. Artificial Neural Network based Solar Energy Integrated Unified Power Quality Conditioner. *Energy Sources Part A Recovery Util. Environ. Eff.* **2021**. [[CrossRef](#)]
29. Fredrick, N.; Franklin, N.; Ifedayo, O.; Ramon, Z. Optimal Design and Performance Analysis of Solar PV Integrated UPQC for Distribution Network. *Eur. J. Electr. Eng. Comput. Sci.* **2021**, *5*, 39–46.
30. Gade, S.; Agrawal, R.; Munje, R. Recent Trends in Power Quality Improvement: Review of the Unified Power Quality Conditioner. *ECTI Trans. Electr. Eng. Electron. Commun.* **2021**, *19*, 268–288. [[CrossRef](#)]
31. Nikita, G.; Seethalekshmi, K. Artificial neural network and synchrosqueezing wavelet transform based control of power quality events in distributed system integrated with distributed generation sources. *Int. Trans. Electr. Energy Syst.* **2021**, *31*, e12824.

32. Nima, K.; Salwa, E.; Rasoul, B.; Zineb, H.; Rahman, H.; Mustapha, M. Enhancement of power quality issues for a hybrid AC/DC microgrid based on optimization methods. *IET Renew. Power Gener.* **2022**, *16*, 1773–1791.
33. Pazhanimuthu, C.; Ramesh, S. Grid integration of renewable energy sources (RES) for power quality improvement using adaptive fuzzy logic controller based series hybrid active power filter (SHAPF). *J. Intell. Fuzzy Syst.* **2018**, *35*, 749–766. [[CrossRef](#)]